Remote Sensing Letters, 2014
Vol. 5, No. 7, 672–681, http://dx.doi.org/10.1080/2150704X.2014.960606

Taylor & Francis
Taylor & Francis Group

Analysis of Landsat-8 OLI imagery for land surface water mapping

Zhiqiang Du[a], Wenbo Li[b]*, Dongbo Zhou[c], Liqiao Tian[a], Feng Ling[d], Hailei Wang[b], Yuanmiao Gui[b], and Bingyu Sun[b]

[a]*State Key Laboratory of Information Engineering in Surveying, Mapping and Remote Sensing, Wuhan University, Wuhan, China;* [b]*Institute of Intelligent Machines, Chinese Academy of Sciences, Hefei, China;* [c]*National Engineering Research Center for E-Learning, Central China Normal University, Wuhan, China;* [d]*Institute of Geodesy and Geophysics, Chinese Academy of Sciences, Wuhan, China*

(*Received 30 November 2013; accepted 26 August 2014*)

The normalized difference water indices (NDWIs) were successfully used in map land surface water mapping (LSWM) from Landsat series multispectral images. This paper evaluates the potential of the recent Landsat satellite (Landsat-8) Operational Land Imager (OLI) multispectral images for LSWM using three NDWI models. We tested the accuracy and robustness of the three OLI NDWI models in the Yangtze River Basin and the Huaihe River Basin in China. The results demonstrate that the three OLI NDWI models achieve an overall accuracy of more than 95%, a kappa coefficient of 0.89 and a producer's accuracy of 95% for LSWM. The results also demonstrate that the NDWI model using the green band (Band 3) and the SWIR1 band (Band 6) (referred to as $NDWI_{O6,3}$) of the OLI sensor has a higher LSWM accuracy than the other two NDWI models.

1. Introduction

Land surface water (LSW), which includes rivers, lakes, reservoirs and wetlands, plays a crucial role in water cycles (Du et al. 2012). Since 1972, the multispectral images from the sensors of the Multispectral Scanner System (MSS, Landsat-1/2/3), Thematic Mapper (TM, Landsat-4/5) and Enhanced Thematic Mapper Plus (ETM+, Landsat-7) have been used to delineate LSW using the methods of single-band density slicing (Ryu, Won, and Min 2002), images classification (Oki, Oguma, and Sugita 2002; Li et al. 2013) and water index (McFeeters 1996; Xu 2006). The Landsat-7 mission was flawless until May 2003. Moreover, a rapidly degrading electronic component ended the Landsat-5 mission in November 2011. Fortunately, the recent Landsat satellite (Landsat-8) launched on 11 February 2013. The potential of the Landsat-8 Operational Land Imager (OLI) images for delineating LSW must be evaluated.

Water indices are better at detecting LSW than single-band density slicing methods (Qiao et al. 2012). Image classification methods are highly dependent on human expertise and have difficulty in producing rapid and reproducible extractions of LSW information because water bodies, such as tides and storm surges, can be fast moving (Ouma and Tateishi 2006). Water indices can extract LSW information more accurately, quickly and easily than classification methods (Li et al. 2013). A commonly used water index is the normalized difference water index (NDWI) (McFeeters 1996). The other widely used water index is the modified NDWI (Xu 2006). McFeeters' NDWI and Xu's NDWI have

*Corresponding author. Email: wbli@iim.ac.cn

been successfully used to delineate LSW information (Li et al. 2013; Feyisa et al. 2014). Therefore, McFeeters' NDWI and Xu's NDWI were used as the primary methods in this study. This paper evaluates the potential of the Landsat-8 OLI images in delineating LSW using different NDWIs so that the data from the Landsat-8 and the other Landsat satellites can be used to map LSW for application purposes, e.g., shoreline extraction, flood area mapping and wetland mapping.

2. Methodology

2.1. Data sites and study sites

Level 1 US Geological Survey (USGS) Landsat-8 OLI images were employed. These images are in the World Geodetic System (WGS84) datum in GeoTIFF format and projected using the Universal Transverse Mercator system. Three OLI images from Landsat-8, which were acquired over the Yangtze River Basin and Huaihe River Basin in China, were used for the LSW mapping (LSWM) analysis. The three OLI images were acquired on 14 May 2013 (path/row 121/38), 13 June 2013 (path/row 123/39) and 14 August 2013 (path/row 125/39). The three study sites contained several water bodies, including small ponds, rivers, reservoirs and lakes, with different environmental conditions such as different depth, turbidity and surface appearances (Figure 1 and Table 1). The sites exhibited predominantly flat or mountainous topography. The test sites were deliberately selected so that the sub-scenes consisted of complex surface features as the background features for the water features. The Dongpu Reservoir was the main water features in Region I, and the background features included the built-up land and vegetation. The Three Gorges Reservoir and the Yangtze River were selected as the main water features in Region II, and the main background features were the Three Gorges Dam, built-up land and vegetation. The Shahu Lake and the Dong Lake were selected as the main water features in Region III, while the main background features were the built-up and vegetation.

It's difficult to obtain accurate ground-truth reference data because the water body changes over time (Ouma and Tateishi 2006). One acceptable option is to use the higher resolution images collected simultaneously with the multispectral images to minimize any

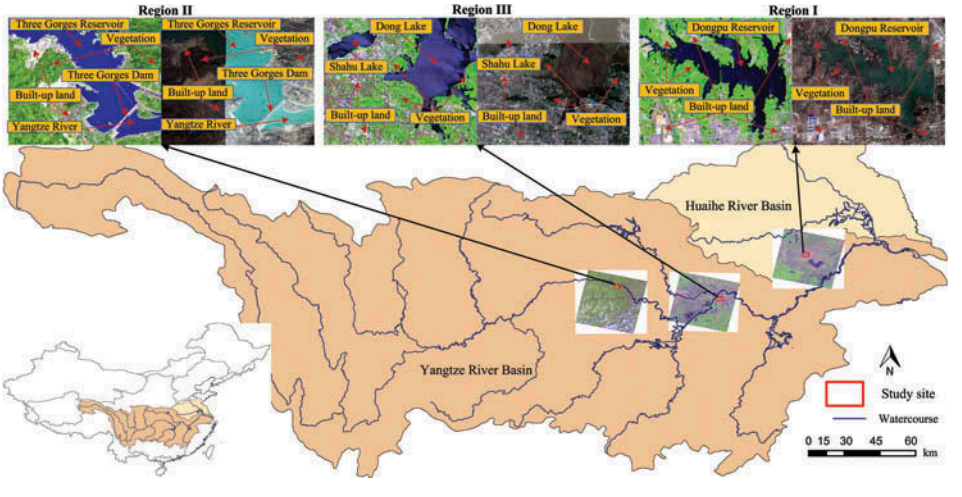

Figure 1. Location of the study area (Image © 2014 Google, DigitalGlobe).

Table 1. Characteristics of the three test sites and corresponding Landsat-8 OLI and reference data.

Test site	General characteristics of the main water	Mean altitude (m)	Topography	Area (ha)	OLI date	Reference points	Reference data and sources
Region I	Clear water of the Dongpu Reservoir	32	Predominantly flat	1500	14 May 2013	Built-up: 6547; Vegetation: 2949; Reservoir: 3408; Pond: 601; Edge: 474	The OLI Pan images at 15 m resolution acquired at the same time as the OLI images. The QuickBird images at 2.4 m resolution provided by Google Earth.
Region II	Clear water of the Three Gorges Reservoir Clear water of the Yangtze River	212	Predominantly mountainous	2160	14 August 2013	Built-up: 1657; Vegetation: 7321; Dam: 738; Reservoir: 2998; River: 495; Edge: 802	
Region III	Turbid water of the Shahu Lake Turbid water of the Dong Lake	30	Predominantly flat	2030	13 June 2013	Built-up: 3020; Vegetation: 6141; Turbid lake: 3288; Edge: 1218	

time-dependent effects. Hence, the 15-m resolution OLI panchromatic images that were acquired at the same time as OLI multispectral images were selected for the ground-truth reference data. We also used the higher resolution QuickBird data (2.4 m) as auxiliary data. The drawback is that QuickBird data downloaded from Google contain differences in terms of their acquisition dates and colours (Figure 1); however, these QuickBird data are sufficient for determining the properties of the random reference points. True ground-truth reference data are preferable if they can be obtained.

2.2. Water indices and data pre-processing

McFeeters' NDWI is a water index which is calculated from (Green-NIR)/(Green+NIR), where Green and NIR are the reflectance of the green and NIR bands (McFeeters 1996). McFeeters' NDWI is unable to completely separate built-up features from water features. To address this problem, the modified NDWI (Xu's NDWI) was developed, which is calculated from (Green-SWIR)/(Green+SWIR), where SWIR is the reflectance of the SWIR band (Xu 2006). In this study, Band 3 (Green) and Band 5 (NIR) of OLI were selected to form one McFeeters' NDWI model, i.e., $NDWI_{O5,3}$,. Moreover, Band 3, Band 6 (SWIR1) and Band 7 (SWIR2) were used to form two Xu's NDWI models, i.e., $NDWI_{O6,3}$ and $NDWI_{O7,3}$. Hence, we must determine which OLI NDWI model performs the best at LSWM.

The parameters used in McFeeters' NDWI and Xu's NDWI require physical quantities, such as the surface reflectance, rather than raw quantized calibrated pixel values. The USGS standard level 1 Landsat-8 OLI products can be rescaled to the surface reflectance using atmospheric correction modules. The FLAASH (Fast Line-of-sight Atmospheric Analysis of Spectral Hypercubes) module can accurately convert the raw quantized calibrated pixel values to surface reflectance (Hu and Tang 2012). We used FLAASH to obtain the surface reflectance values of the OLI data in this study. The following equations are used in FLAASH:

$$L = \mathrm{A}\frac{\rho}{1 - \mathrm{S}\rho_e} + \mathrm{B}\frac{\rho_e}{1 - \mathrm{S}\rho_e} + L_a \tag{1}$$

where L is the pixel spectral radiance, ρ is the pixel surface reflectance, ρ_e is the averaged surface reflectance, S is the atmosphere spherical albedo, L_a is the radiance backscattered by the atmosphere. The parameters A, B, S and L_a are calculated from the FLAASH module contained in the ENVI software package 5.0 provided by Envirosphere Company (Redlands, CA, USA).

Furthermore, L can be obtained from the raw quantized calibrated pixel values (Q_{cal}) as follows:

$$L = \mathrm{M}Q_{cal} + \mathrm{A} \tag{2}$$

where M is the band-specific multiplicative rescaling factor and A is the band-specific additive rescaling factor. The parameters M and A are included in the OLI metadata file (MTL file).

2.3. Image threshold segmentation

The thresholds for McFeeters' NDWI and Xu's NDWI were set to zero; however, adjusting the threshold can more accurately delineate LSW information (Ji, Zhang, and

Wylie 2009). The Otsu method (Otsu 1979) has been used successfully in LSW detection (Du et al. 2012; Li et al. 2013). Therefore, the Otsu method was used in this study. The Otsu method uses the maximum between-class variance criterion to determine the optimal threshold t^* for NDWI image segmentation:

$$\begin{cases} \sigma^2 = P_{nw} \cdot (M_{nw} - M)^2 + P_w \cdot (M_w - M)^2 \\ M = P_{nw} \cdot M_{nw} + P_w \cdot M_w \\ P_{nw} + P_w = 1 \\ t* = Arg \underset{a \le t \le b}{Max} \left\{ P_{nw} \cdot (M_{nw} - M)^2 + P_w \cdot (M_w - M)^2 \right\} \end{cases} \tag{3}$$

where σ is the between-class variance of the non-water and water, M is NDWI image mean value, P_{nw} is the non-water class probability, P_w is the water class probability, M_{nw} is the non-water class mean value and M_w is the water class mean value. Additional details of the Otsu method for NDWI image segmentation can be found in Li et al. (2013).

2.4. *Water body mapping validation*

We used the producer's accuracy (PA), overall accuracy (OA) and kappa coefficient to evaluate the accuracy and robustness of the three OLI NDWI models at three sites. Additional details of PA, OA and kappa coefficient can be obtained from Foody's (2002) results. The assessment was performed in three steps. First, we selected the OLI panchromatic and QuickBird images with 2.4-m spatial resolution as the reference data. Second, we used the OLI panchromatic images to generate more than 12,000 reference points. To ensure the representativeness, more than 4000 random water features and background features points were selected, respectively. In Region I, the 9496 background features reference points represented built-up (6547 points) and vegetation (2949 points), while the 4483 water features reference points represented ponds (601 points), the edge of the Dongpu Reservoir (474 points) and the middle of the Dongpu Reservoir (3408 points). The details of the reference points for Region II and Region III can be found from Table 1. We then used the reference points to assess the accuracy of OLI LSW maps.

3. Results and discussions

The contrast between the water and the background was clear (Figure 1) at the three test sites. A visual interpretation indicates that the nine NDWI images (Figures 2(*a*), (*d*), (*g*), 3(*a*), (*d*), (*g*), 4(*a*), (*d*), and (*g*)) clearly displayed open water bodies due to the enhancement process. We used zero as the threshold to obtain the nine LSW maps (Figures 2(*b*), (*e*), (*h*), 3(*b*), (*e*), (*h*), 4(*b*), (*e*), and (*h*)). The Otsu method determined thresholds (Table 2) were applied to obtain the nine LSW maps (Figures 2(*c*), (*f*), (*i*), 3(*c*), (*f*), (*i*), 4(*c*), (*f*), and (*i*)). The visual interpretation also indicates that the nine LSW maps, derived from the zero threshold, contained many misclassifications, especially in Figures 2(*h*), 3(*h*) and 4(*h*), which were all derived from the $NDWI_{O7,3}$ image.

3.1. *Land surface water mapping accuracy analysis*

A visual interpretation indicates that the nine LSW maps derived from the Otsu method performed better than the nine LSW maps that used zero as the thresholds. Thus, we used the PA, OA and kappa coefficient to quantitatively assess the accuracy of the nine

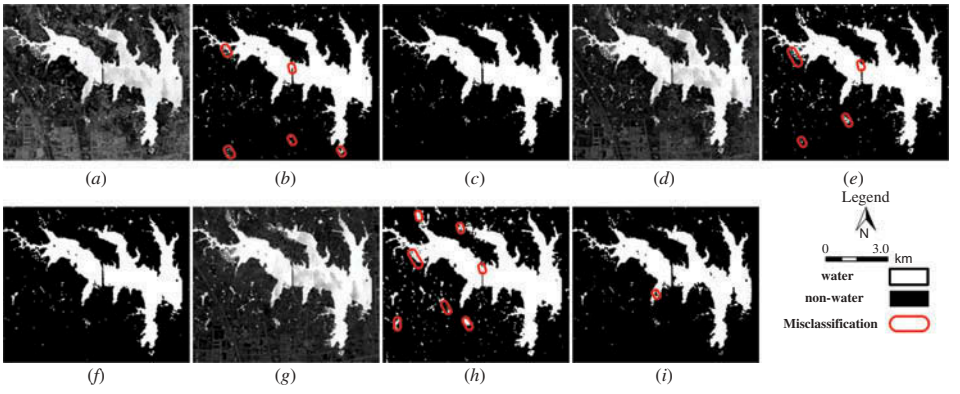

Figure 2. Comparison of the resulting LSW maps derived from Landsat-8 OLI imagery in Region I. (*a*) OLI $NDWI_{O5,3}$ image; (*b*) LSW map of $NDWI_{O5,3}$ with a 0.0 threshold; (*c*) LSW map of $NDWI_{O5,3}$ with a 0.238 threshold; (*d*) OLI $NDWI_{O6,3}$ image; (*e*) LSW map of $NDWI_{O6,3}$ with a 0.0 threshold; (*f*) LSW map of $NDWI_{O6,3}$ with a 0.343 threshold; (*g*) OLI $NDWI_{O7,3}$ image; (*h*) LSW map of $NDWI_{O7,3}$ with a 0.0 threshold; and (*i*) LSW map of $NDWI_{O7,3}$ with a 0.525 threshold.

LSW maps derived from the Otsu method in this section. Three scenarios were designed to analyse the accuracy of the NDWI models at depicting different types of water bodies and zones. The scenarios of all water features, which included the reference points of middle water features and the edges of water features, were used to assess the total accuracy of the LSW maps. The middle water features scenarios, which used the reference points for the main water features, were used to assess the accuracy of the larger water features. Moreover, the scenarios of water body edge features, which used the reference points for the edges of water features (e.g., water–land boundaries) and smaller water features (e.g., small ponds), were used to assess the accuracy of small water features.

The total accuracy of the nine LSW maps (three 'all' columns in Table 2) is relatively stable in the three test regions. The PA, OA and kappa coefficient values for the total accuracy of the nine LSW maps exceeded 85%, 94% and 0.85, respectively. The highest PA, OA and kappa coefficient values for the LSW maps at the three test sites corresponded to the maps generated using the $NDWI_{O6,3}$ model. The accuracy of larger water features (three 'middle' columns in Table 2) at the three test sites exceeded the total accuracy of the nine LSW maps. The PA, OA and kappa coefficient values for the larger water features exceeded 95%, 95% and 0.92; the maximum PA, OA and kappa coefficient values were obtained using the $NDWI_{O6,3}$ model. In the water body edge scenario (three 'edge' columns in Table 2), the OA values for the three test sites exceeded 93%; however, the PA and kappa coefficient values were smaller than those obtained for the other two scenarios. Moreover, the highest PA and kappa coefficient values were only 80.92% and 0.8432, both coming from the $NDWI_{O6,3}$ LSW map in Region II. The smallest PA and kappa coefficient values were 41.49% and 0.5535, respectively, which were for the $NDWI_{O7,3}$ LSW map in Region I. However, the highest PA, OA and kappa coefficient values were still obtained using the $NDWI_{O6,3}$ model under the condition of small water features and near the edge of water bodies.

The results (Table 2) illustrate that the OLI $NDWI_{O6,3}$ model consistently had the highest performance of the three NDWI models for LSWM at the three study sites under the three different scenarios. The detailed analysis presented earlier indicates that utilizing

Table 2. Summary of the classification accuracy of the three NDWI models according to the three test sites.

			Producer's accuracy (%)			Overall accuracy (%)			Kappa coefficient		
Place	NDWI	Threshold	All	Middle	Edge	All	Middle	Edge	All	Middle	Edge
Region I	$NDWI_{O5,3}$	0.238	86.48	98.97	46.88	95.56	99.61	94.46	0.8944	0.9900	0.6063
	$NDWI_{O6,3}$	0.343	88.02	99.18	52.65	96.03	99.64	95.01	0.9060	0.9908	0.6578
	$NDWI_{O7,3}$	0.525	86.21	95.22	41.49	95.45	98.62	93.91	0.8919	0.9640	0.5535
Region II	$NDWI_{O5,3}$	0.113	95.66	99.57	78.68	97.97	99.14	97.44	0.9520	0.9781	0.8105
	$NDWI_{O6,3}$	0.286	96.01	99.48	80.92	98.29	99.35	97.90	0.9595	0.9833	0.8432
	$NDWI_{O7,3}$	0.462	93.84	99.34	69.95	97.74	99.43	97.21	0.9461	0.9854	0.7783
Region III	$NDWI_{O5,3}$	−0.052	89.75	97.45	68.97	94.51	97.00	93.56	0.8745	0.9244	0.6796
	$NDWI_{O6,3}$	0.029	91.90	98.54	73.97	95.41	97.51	94.42	0.8956	0.9372	0.7253
	$NDWI_{O7,3}$	0.060	95.16	99.39	83.74	94.29	95.88	93.34	0.8841	0.8987	0.7092

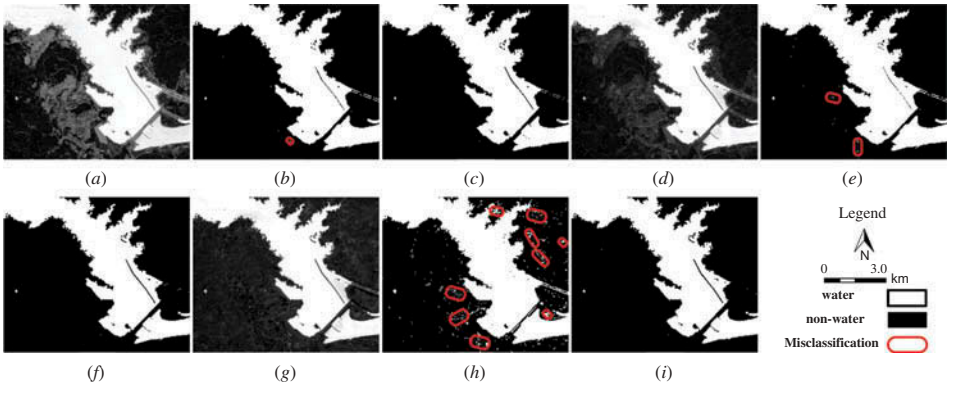

Figure 3. Comparison of the resulting LSW maps derived from Landsat-8 OLI imagery in Region II. (*a*) OLI $NDWI_{O5,3}$ image; (*b*) LSW map of $NDWI_{O5,3}$ with a 0.0 threshold; (*c*) LSW map of $NDWI_{O5,3}$ with a 0.113 threshold; (*d*) OLI $NDWI_{O6,3}$ image; (*e*) LSW map of $NDWI_{O6,3}$ with a 0.0 threshold; (*f*) LSW map of $NDWI_{O6,3}$ with a 0.286 threshold; (*g*) OLI $NDWI_{O7,3}$ image; (*h*) LSW map of $NDWI_{O7,3}$ with a 0.0 threshold; and (*i*) LSW map of $NDWI_{O7,3}$ with a 0.462 threshold.

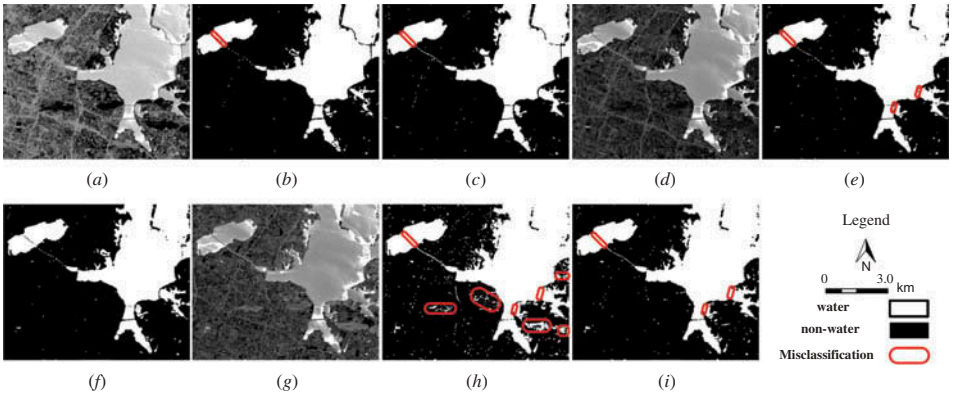

Figure 4. Comparison of the resulting LSW maps derived from Landsat-8 OLI imagery in Region III. (*a*) OLI $NDWI_{O5,3}$ image; (*b*) LSW map of $NDWI_{O5,3}$ with a 0.0 threshold; (*c*) LSW map of $NDWI_{O5,3}$ with a −0.052 threshold; (*d*) OLI $NDWI_{O6,3}$ image; (*e*) LSW map of $NDWI_{O6,3}$ with a 0.0 threshold; (*f*) LSW map of $NDWI_{O6,3}$ model with a 0.029 threshold; (*g*) OLI $NDWI_{O7,3}$ image; (*h*) LSW map of $NDWI_{O7,3}$ with a 0.0 threshold; and (*i*) LSW map of $NDWI_{O7,3}$ with a 0.060 threshold.

the green band (Band 3, at wavelengths of 0.53–0.59 μm) and the SWIR1 band (Band 6, at wavelengths of 1.57–1.65 μm) of the OLI to form Xu's NDWI is the optimal choice for LSWM. This result is consistent with laboratory analyses of spectral data (Ji, Zhang, and Wylie 2009), which show that the NDWI model that uses the green band and SWIR band (at wavelengths of 1.2–1.8 μm) is suitable for delineating LSW.

The results demonstrate that the $NDWI_{O6,3}$ and $NDWI_{O5,3}$ models are more suitable for mapping LSW than the $NDWI_{O7,3}$ model, even for small water features. The results demonstrates that the OLI $NDWI_{O7,3}$ model can also be used for LSWM. The $NDWI_{O7,3}$ model is suitable for mapping large water features such as the large reservoirs in Region II and the large lake in Region III. However, the OLI $NDWI_{O7,3}$ model poorly maps small

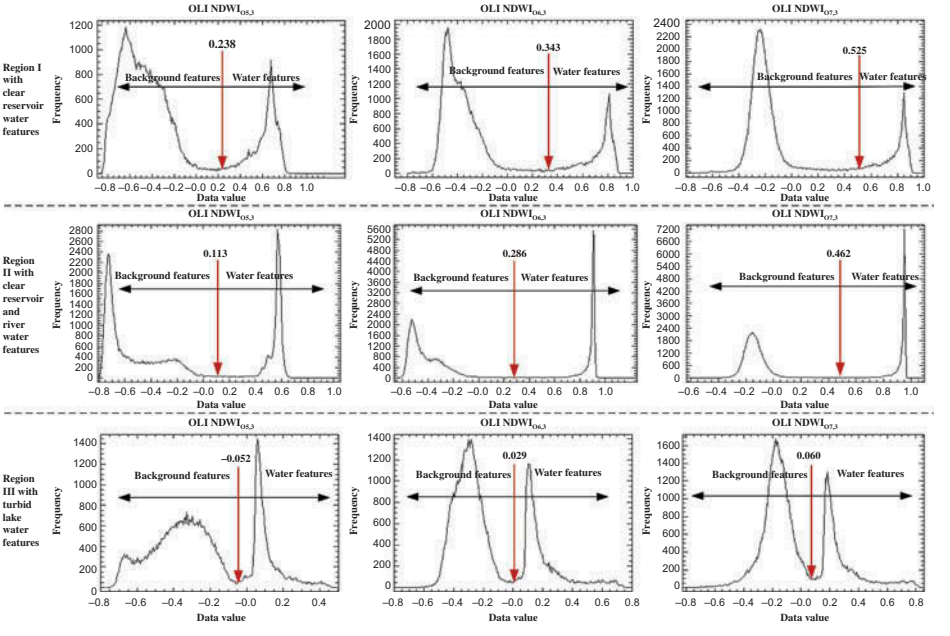

Figure 5. Comparison of the histograms and optimal thresholds (marked with a red arrow) for the three NDWI models using the Landsat-8 OLI data.

water features such as the ponds in Region I. The results also demonstrate that there were a few misclassifications, especially for small water features and eater body edges, in the LSW maps that were caused by an overestimation of small water features (e.g., certain small ponds in Region I) and mixed land–water pixels (e.g., water–land boundaries in the three test regions). These problems can be addressed using a spectral unmixing technique (Oki, Oguma, and Sugita 2002).

3.2. *Optimal segmentation threshold analysis*

Threshold selection is very important in LSWM using McFeeters' NDWI and Xu's NDWI. The NDWI image histograms are bimodal (Figure 5). The critical threshold can be used for LSWM. The determined thresholds using Otsu method are at the bottoms of the two peaks (Figure 5). Previous work has shown that larger variances between the water features and background features typically minimize the probability of LSW (Li et al. 2013). The maximum variance values between the features of water and background for the three OLI NDWI models at the three test sites were derived from the $NDWI_{O6,3}$ image, which also indicates that the OLI $NDWI_{O6,3}$ model has more robustness for LSWM than the $NDWI_{O5,3}$ and $NDWI_{O7,3}$. This result is consistent with the results of the LSWM accuracy analysis.

4. Conclusions

In this study, we evaluated the potential of the Landsat-8 OLI images for LSWM. We calculated three OLI NDWI models for LSWM in the Yangtze River Basin and the Huaihe River Basin, China. The results demonstrate that the OLI images can be accurately and easily used for LSWM. The results also demonstrate that the $NDWI_{O6,3}$ model based on the green band (Band 3) and the SWIR1 band (Band 6) of the OLI is the best indicator

for LSWM. The results also demonstrate that using green and SWIR1 bands of the OLI sensor to derive Xu's NDWI provides better LSWM results than using McFeeters' NDWI, which is consistent with previous results (Xu 2006; Ji, Zhang, and Wylie 2009). These results indicate that the new Landsat satellite data from the OLI sensor can be used to delineate LSW information with other Landsat images such as TM and ETM+.

Acknowledgements

We are indebted to USGS server (http://earthexplorer.usgs.gov/).

Funding

This study was financially supported by the National Natural Science Foundation of China [grant number 41171311, 41101516 and 41201413].

References

Du, Z., B. Linghu, F. Ling, W. Li, W. Tian, H. Wang, Y. Gui, B. Sun, and X. Zhang. 2012. "Estimating Surface Water Area Changes Using Time-Series Landsat Data in the Qingjiang River Basin, China." *Journal Applied Remote Sensing* 6: 063609. doi:10.1117/1.JRS.6.063609.

Feyisa, G. L., H. Meilby, R. Fensholt, and S. R. Proud. 2014. "Automated Water Extraction Index: A New Technique for Surface Water Mapping Using Landsat Imagery." *Remote Sensing of Environment* 140: 23–35. doi:10.1016/j.rse.2013.08.029.

Foody, G. M. 2002. "Status of Land Cover Classification Accuracy Assessment." *Remote Sensing of Environment* 80: 185–201. doi:10.1016/S0034-4257(01)00295-4.

Hu, C., and P. Tang. 2012. "Automatic Algorithm for Relative Radiometric Normalization of Data Obtained from Landsat TM and HJ-1A/B Charge-Coupled Device Sensors." *Journal Applied Remote Sensing* 6. doi:10.1117/1.jrs.6.063509.

Ji, L., L. Zhang, and B. Wylie. 2009. "Analysis of Dynamic Thresholds for the Normalized Difference Water Index." *Photogrammetric Engineering & Remote Sensing* 75: 1307–1317. doi:10.14358/PERS.75.11.1307.

Li, W., Z. Du, F. Ling, D. Zhou, H. Wang, Y. Gui, B. Sun, and X. Zhang. 2013. "A Comparison of Land Surface Water Mapping Using the Normalized Difference Water Index from TM, ETM+ and ALI." *Remote Sensing* 5: 5530–5549. doi:10.3390/rs5115530.

McFeeters, S. K. 1996. "The Use of the Normalized Difference Water Index (NDWI) in the Delineation of Open Water Features." *International Journal of Remote Sensing* 17: 1425–1432. doi:10.1080/01431169608948714.

Oki, K., H. Oguma, and M. Sugita. 2002. "Subpixel Classification of Alder Trees Using Multitemporal Landsat Thematic Mapper Imagery." *Photogrammetric Engineering & Remote Sensing* 68: 77–82. http://asprs.org/a/publications/pers/2002journal/january/2002_jan_77-82.pdf.

Otsu, N. 1979. "A Threshold Selection Method from Gray-Level Histograms." *IEEE Transactions on Systems, Man, and Cybernetics* 9: 62–66. doi:10.1109/TSMC.1979.4310076.

Ouma, Y. O., and R. Tateishi. 2006. "A Water Index for Rapid Mapping of Shoreline Changes of Five East African Rift Valley Lakes: an Empirical Analysis Using Landsat TM and ETM+ Data." *International Journal of Remote Sensing* 27: 3153–3181. doi:10.1080/01431160500309934.

Qiao, C., J. Luo, Y. Sheng, Z. Shen, Z. Zhu, and D. Ming. 2012. "An Adaptive Water Extraction Method from Remote Sensing Image Based on NDWI." *Journal of the Indian Social Remote Sensing* 40: 421–433. doi:10.1007/s12524-011-0162-7.

Ryu, J. H., J. S. Won, and K. D. Min. 2002. "Waterline Extraction from Landsat TM Data in a Tidal Flat: A Case Study in Gomso Bay, Korea." *Remote Sensing of Environment* 83: 442–456. doi:10.1016/S0034-4257(02)00059-7.

Xu, H. 2006. "Modification of Normalised Difference Water Index (NDWI) to Enhance Open Water Features in Remotely Sensed Imagery." *International Journal of Remote Sensing* 27: 3025–3033. doi:10.1080/01431160600589179.